

Effect of N and Al Doping on 3C-SiC Stacking Faults

Cristiano Calabretta^{1,a*}, Viviana Scuderi^{1,b}, Ruggero Anzalone^{2,c},
Annalisa Cannizzaro^{1,d}, Marco Mauceri^{3,e}, Danilo Crippa^{4,f},
Simona Boninelli^{1,g} and Francesco La Via^{1,h}

¹CNR-IMM, VIII Strada, 5, 95121 Catania, Italy

²STMicroelectronics, Stradale Primosole 50, 95121
Catania, Italy

³LPE, Strada XVI, Catania, Italy

⁴LPE, via Falzarego 8 Baranzate (MI), Italy

^{a*}cristiano.calabretta@imm.cnr.it, ^bviviana.scuderi@imm.cnr.it, ^cruggero.anzalone@st.com,
^dannalisa.cannizzaro@imm.cnr.it, ^emarco.mauceri@lpe-epi.com, ^fdanilo.crippa@lpe-epi.com,
^gsimona.boninelli@imm.cnr.it, ^hfrancesco.lavia@imm.cnr.it

Keywords: 3C-SiC; Stacking Faults; doping; Al; Ni; defect; KOH etching; SEM; μ -Raman.

Abstract. This study offers a comprehensive examination of the behavior of 3C-SiC crystals grown on 4° off-axis (100) Si substrates with different off-axis angles along $\langle 110 \rangle$ and $\langle 100 \rangle$ for N and Al doping, respectively. The investigation takes advantage of molten KOH etching to conduct an in-depth investigation of the average density and size of the SFs inside the crystal for both n- and p-type doped 3C-SiC epitaxial layers. Moreover, 3C-SiC grown on a $\langle 100 \rangle$ off-cut substrate was revealed to have a greater concentration of SFs due to the absence of self-annihilation along the plane (-1-10). Considering two different doping ranges suitable for IGBTs and MOSFETs development, the impact of doping and off-angle on the crystal quality, concentration, and length distribution of SFs was then investigated in order to quantify the influence of N and Al incorporation on the structural and optical characteristics of the semiconductor. It turned out that under heavy nitrogen doping ($\sim 10^{19} \text{ cm}^{-3}$), when the dopant concentration grew, the average length of the stacking faults (SFs) expanded while their density dropped.

Introduction

Due to its higher mobility and a lower electronic density of states at the 3C-SiC/SiO₂ junction compared to 4H-SiC, 3C-SiC reveals itself as a remarkable SiC polytype. These properties, resulting from the higher symmetry due to lower phonon scattering and lower bandgap (2.5 eV), make 3C-SiC ideal for applications in power electronics [1], since they provide numerous benefits in metal oxide semiconductor (MOS) devices and microelectromechanical systems (MEMS) in harsh environments [2]. 3C-SiC can be grown by heteroepitaxial growth on Si wafers. However, this type of CVD growth involves 20% of the lattice parameter mismatch between SiC and Si as well as an 8% difference in thermal expansion coefficient. Such mismatches contribute to the generation of SFs lying on the (111) planes as well as misfit dislocations at the interface with Si substrate [3-5]. Doping is known to influence both the crystalline and mechanical properties of semiconductors. It is therefore of interest to verify its action on 3C-SiC [6]. Both μ -Raman and SFs assessment through molten KOH etching were conducted on various doped samples, in order to evaluate the impact of N and Al incorporation on the structural and optical characteristics of the semiconductor. The concentrations examined in this study ($\sim 10^{18} \text{ cm}^{-3}$ for Al and $\sim 10^{19} \text{ cm}^{-3}$ for N) are consistent with the doping levels required for many power devices on 3C-SiC.

Specifically, for vertical metal-oxide-semiconductor field-effect transistor (MOSFET) devices, the substrate concentration should be as high as 10^{19} cm^{-3} in order to reduce the device R_{on} state resistance. Instead, the p-collector of insulated gate bipolar transistors (IGBTs) is characterized by a

concentration of approximately 10^{18} cm^{-3} [7]. Today, IGBT manufacturing is particularly costly due to the difficulty to grow 4H-SiC p-doped wafers, whereas this issue could be avoided by relying on heteroepitaxial growths of 3C-SiC. Consequently, in this work p and n doping were carried out with the above mentioned concentration required for the design of the IGBT and MOSFET. For the two types of doping, two alternative 4° off-axis substrate orientations were used: $\langle 110 \rangle$ and $\langle 100 \rangle$. Using the two intrinsic growths as a benchmark, it was possible to state that, regardless of the type of doping, 3C-SiC growth on $\langle 110 \rangle$ oriented Si substrate succeeds in efficiently close the $(-1-11)$ SFs family, whereas the off-axis angle $\langle 100 \rangle$ results in higher SFs generation and propagation.

Materials and Methods

3C-SiC was grown in a horizontal hot-wall CVD reactor, on (100) oriented Si substrates 4° off-axis along the $\langle 110 \rangle$ for N doped samples and 4° off-axis along the $\langle 100 \rangle$ for Al doped samples. Precursor gases were Tri-chloro-silane (TCS) and Ethylene (C_2H_4) with (H_2) employed as carrier gas. A two-step growth process was applied with the carbonization plateau at 1160°C followed by CVD growth step at 1400°C . A group of 4-inch wafer was grown with 313, 800 and 1600 sccm N_2 fluxes during growth, while another one with constant 1,2,4 sccm Trimethylaluminum (TMA) fluxes. To increase crystal quality, the growth was first performed at $3 \mu\text{m/h}$ for 30', followed by another 30' growth at $6 \mu\text{m/h}$ and then carrying on at $30 \mu\text{m/h}$ until a $70 \mu\text{m}$ layer was reached. Si substrate was then melted at 1600°C inside the reactor to reach a free-standing wafer. Two different intrinsic samples were also grown on $\langle 110 \rangle$ and $\langle 100 \rangle$ off-cut substrate directions with the above mentioned steps in order to cross check the contributions of both the off-cut direction and of the concentration of dopant incorporated in 3C-SiC on crystal quality. From Secondary Ion Mass Spectroscopy (SIMS) analysis the three TMA fluxes led respectively to Al concentration as high as 1.7×10^{18} , 3.4×10^{18} and $6.8 \times 10^{18} \text{ cm}^{-3}$, while N_2 fluxes resulted in concentrations of 1.2×10^{19} , 2.9×10^{19} , $5.8 \times 10^{19} \text{ cm}^{-3}$. Micro-Raman spectroscopy was used to assess 3C-SiC crystal quality. SFs evaluation was carried out through molten KOH etching performed at 500°C for 3' and subsequent SEM analysis.

Discussion

Through in-plane μ -Raman analysis it was attested how the investigated Al concentration exhibits an increase in Transverse Optic (TO) mode FWHM of $\sim 1 \text{ cm}^{-1}$ in the highest doped sample with respect to the intrinsic 3C-SiC relative value. The N incorporation, on the other hand, displays a different behavior, as shown in Fig. 1a.

High N doping induces progressive crystal quality improvement through N_2 flow rise in chamber, as demonstrated by the FWHM dropping of Raman TO mode to $7.4 \pm 1.0 \text{ cm}^{-1}$ in $5.8 \times 10^{19} \text{ cm}^{-3}$ doped sample. Selective KOH etching was employed to perform SFs density evaluation. Fig. 1b displays three SEM micrographs related to the intrinsic and $5.8 \times 10^{19} \text{ cm}^{-3}$ N doped sample grown on $\langle 110 \rangle$ off-cut 4° off-axis substrate and $3.4 \times 10^{18} \text{ cm}^{-3}$ Al doped sample grown on $\langle 100 \rangle$ off-cut 4° off-axis substrate after molten KOH etching process. The presence of SFs is highlighted by the wet etching process due to the difference in etching speed established by the altered binding energy between the defect-free crystalline matrix and the faulted crystal. This facilitates the generation of grooves around the SFs, making them accessible to statistical investigation. As may be observed, the density of SFs is in accordance with the Raman trend depicted in Fig. 1a.

Fig. 2 shows a significant change in the concentration and medium size of SFs between the intrinsic and the highly doped sample. Al doped sample exhibit SFs concentration ranging from $5.7 \times 10^3 \text{ cm}^{-1}$ for $1.7 \times 10^{18} \text{ cm}^{-3}$ to $4.1 \times 10^3 \text{ cm}^{-1}$ for the sample with $3.4 \times 10^{18} \text{ cm}^{-3}$ doping, attaining a slight reduction only to $4.7 \times 10^3 \text{ cm}^{-1}$ for the highest Al doping level (Fig. 2a). In the case of N

doping, instead, SFs density shows a different trend; it is, in fact, evident that if for the intrinsic off axis sample the average SFs density is $2.05 \times 10^3 \text{ cm}^{-1}$, by increasing N doping to $2.9 \times 10^{19} \text{ cm}^{-3}$ and $5.8 \times 10^{19} \text{ cm}^{-3}$, such value is notably reduced by almost an order of magnitude to $4.7 \times 10^2 \text{ cm}^{-1}$ and $2.4 \times 10^2 \text{ cm}^{-1}$ and has been proven to be independent from N saturation threshold [8] in 3C-SiC crystalline matrix.

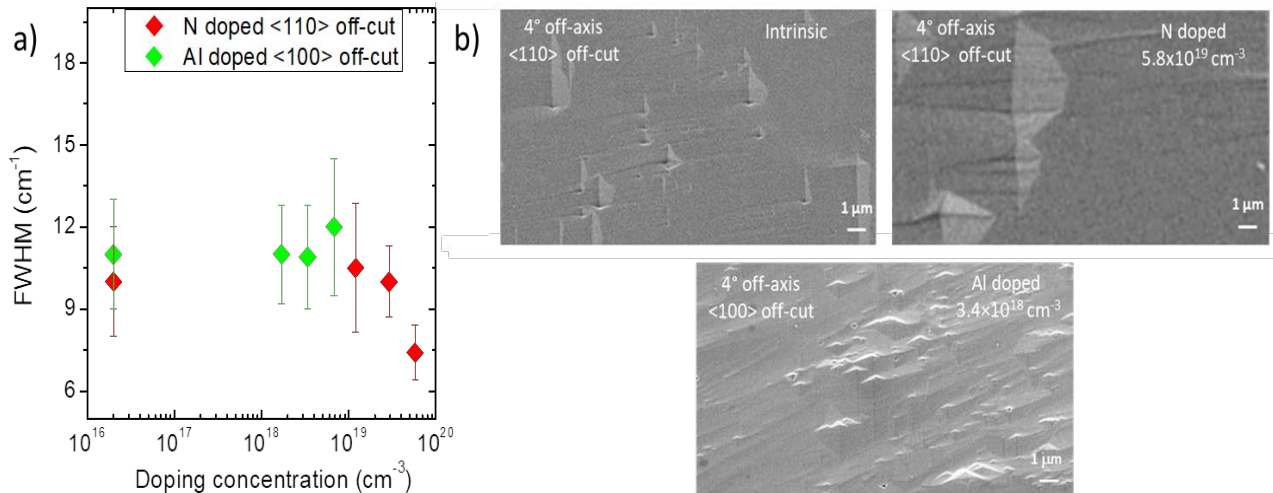


Figure 1. a) 3C-SiC TO mode FWHM for Al and N doped samples; b) SEM micrograph of intrinsic N and Al doped samples after molten KOH etching.

This result is consistent with ab initio Density Functional Theory (DFT) calculation, which establishes that nitrogen doping around a SF increases its formation energy [9] and, thus, suppresses the SF formation. The medium length values in N-type doping are larger than the value of the intrinsic off-axis with <110> off-cut direction. In comparison with the Al doping, the lowered SFs concentration is susceptible to a less effective mechanism of mutual annihilation and contributes to SFs average size increase from $1.8 \pm 1.4 \text{ μm}$ to $5.2 \pm 2.6 \text{ μm}$ (Fig. 2b).

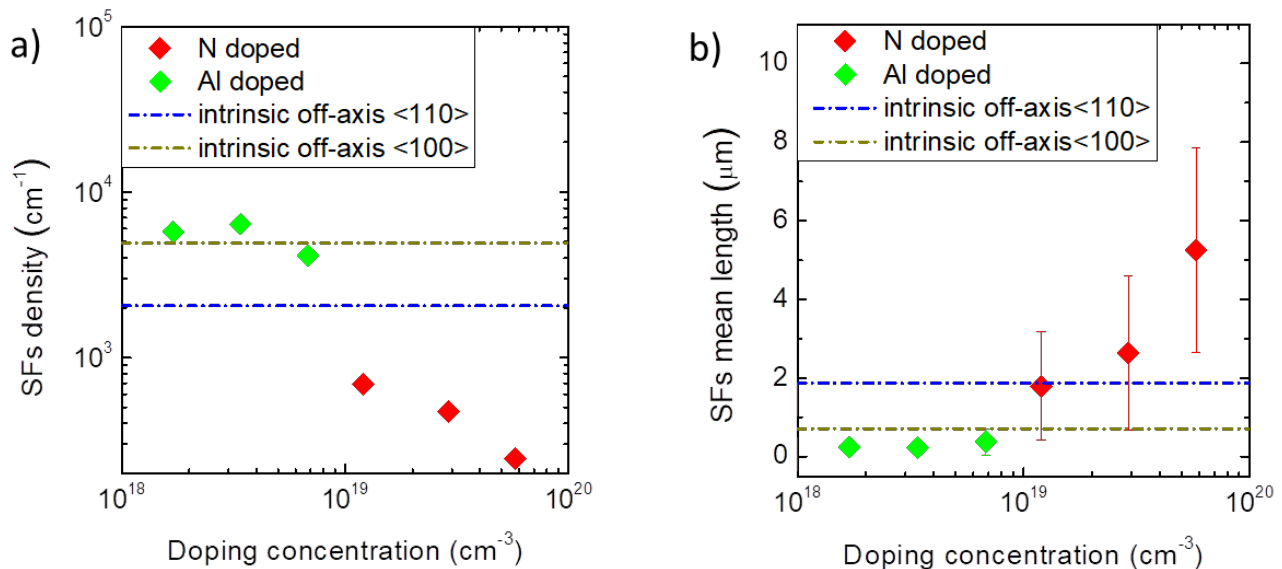


Figure 2. a) SFs density b) SFs mean length of P and Al doped 3C-SiC epitaxial layers. The graphs report the data related to intrinsic samples under different <110> and <100> off-cuts.

The <110> off-axis direction of Si substrates favors propagation up to the surfaces of the SFs lying along the plane (111), whereas the SF lying on (-1-11) opposite to the growth step are prohibited [10]. Indeed Fig. 2a exhibits how the orientation of the off-axis angle introduces a consistent variation in the concentration of SFs already between intrinsic heteroepitaxies. The

off-axis angle in n-type samples is in the $\langle 110 \rangle$ direction, favoring the inhibition of SFs along the plane $(-1-11)$. The off-axis angle for p-type samples is along the $\langle 100 \rangle$ direction and does not avoid SFs propagation from $(-1-11)$. As a result, the SFs lying along the $(-1-11)$ are fully removed only in n-type sample off-cut direction. In conclusion the association of current doping systems alongside compliance substrates adoption, such as inverted Silicon pyramids [11] or $\text{Si}_{1-x}\text{Ge}_x$ buffer layer [12] could further implement growth strategies in order to reduce the concentration of SFs and leading to the development of efficient 3C-SiC power devices.

Acknowledgements

This research was funded by SiC Nano for PicoGeo project, European Union's Horizon 2020 research and innovation programme under grant agreement No. 863220.

Summary

N and Al doped 3C-SiC heteroepitaxial layers, were grown on a Si (100) substrate in a horizontal hot-wall CVD reactor. Samples were grown on Si (100) 4° off-axis along $\langle 110 \rangle$ and $\langle 100 \rangle$ for N and Al doped samples with two doping ranges, respectively. In the case of N-type doping, it was discovered that, as the dopant concentration increases, the mean length of the SFs grows from 2 μm to 5 μm , but the density drops. Instead, when the doping concentration is increased in p-type doping, the mean length and density of the SFs stay almost unchanged. Both quantities (density and average length) are influenced by the cutting angle's orientation. In reality, the off-axis angle along the $\langle 110 \rangle$ promotes the suppression of the SFs along the plane $(-1-11)$, lowering the density of the SFs detected on surface and expanding their average length. Conversely, not all of the SFs along the plane $(-1-11)$ were suppressed on $\langle 100 \rangle$ off-cut. This increases the reciprocal annihilation process, which is able of decreasing the average lengths of the SFs on the surface.

References

- [1] M. Willander, Silicon carbide and diamond for high temperature device applications. J. Mater. Sci. Mater. Electron. 2006, 17, 1–25.
- [2] R.G. Azeved, A SiC MEMS resonant strain sensor for harsh environment applications. IEEE Sens. J., 7, 2007, 568–576.
- [3] F. La Via et al. New approaches and understandings in the growth of cubic silicon carbide, Materials, 14(18), 2021, 5348.
- [4] M. Zimbone et al., Generation and Termination of Stacking Faults by Inverted Domain Boundaries in 3C-SiC, Crystal Growth and Design, 20(5), 2020, 3104-3111.
- [5] M. Zimbone et al. Extended defects in 3C-SiC: Stacking faults, threading partial dislocations, and inverted domain boundaries, Acta Materialia, 213, 2021, 116915.
- [6] V. Scuderi et al. Characterization of 4H- and 6H-like stacking faults in cross section of 3C-SiC epitaxial layer by room-temperature μ -photoluminescence and μ -Raman analysis, Materials, 13(8) 2020, 1837.
- [7] Li, R.; Huang, et al. carrier-storage-enhanced superjunction IGBT with n-Si and p-3C-SiC pillars. Electron. Lett., 55, 2019, 1353–1355.
- [8] F. Li, Y. Sharma, Vishal Shaha, et al., App. Surf. Science, 353, 958–963, (2015)
- [9] Y. Umeno, K. Yagi, and H. Nagasawa, Phys. Status Solidi B, 1–6, (2012).

- [10] C. Calabretta, et al. Effect of Nitrogen and Aluminum Doping on 3C-SiC Heteroepitaxial Layers Grown on 4° Off-Axis Si (100), *Materials*, 14(16), 2021, 4400.
- [11] M. Zimbone et al. 3C-SiC growth on inverted silicon pyramids patterned substrate, *Materials*, 2019, 3407.
- [12] M. Zimbone, M. Zielinski, C. Bongiorno et al 3C-SiC growth on inverted silicon pyramids patterned substrate, *Materials*, 12(20), 2019, 3407.